Balaguer-Beser *et al. Fire Ecology* (2026) 22:46
https://doi.org/10.1186/s42408-026-00470-y

Fire Ecology

Association for Fire Ecology

RESEARCH

Open Access

Altitudinal variation in fire behavior in Andean ecosystems in southern Ecuador

Angel Balaguer-Beser[1*], Fernando González[2], Carlos G. Chuncho[3], Vinicio Carrión-Paladines[4] and Oscar Juela-Sivisaca[5]

Abstract

Background Wildfires constitute an increasingly significant ecological disturbance in Andean ecosystems, particularly in high-elevation shrublands and páramo transition zones. In southern Ecuador, recent increases in fire activity underscore the need to better understand how fire behavior responds to steep elevation gradients, where fuel characteristics, microclimate, and topography vary over short distances. This study examined fire behavior during controlled burns across three contrasting elevational zones (1549–2757 m a.s.l.) to identify the primary ecological and environmental controls on rate of spread, flame length, flame height, and soil temperature at a depth of 5 cm.

Results Fire behavior varied systematically along the elevation gradient, reflecting shifts in the dominant ecological constraints on combustion. At higher elevations with steep slopes, wind exposure, and terrain–wind interactions favored faster spread and greater flame development. At mid elevations, where slopes are moderate, vegetation moisture limited spread and flame development, indicating that live-fuel water status strongly regulates flammability even under moderate atmospheric forcing. At lower elevations, gently sloping shrublands, higher solar radiation and greater surface dryness were associated with more variable fire behavior, consistent with a fragmented fuel structure and heterogeneous fuel continuity. These patterns indicate that elevation gradient does not simply scale fire intensity but reorganizes the balance among topographic forcing, atmospheric conditions, and fuel properties.

Conclusions Fire behavior in Andean landscapes is governed by shifting ecological controls along elevation, rather than by a single dominant driver. Recognizing these zone-specific mechanisms can strengthen Integrated Fire Management by aligning prevention, monitoring, and risk-reduction strategies with the ecological context of each elevational zone.

Keywords Wildfires, Fire behavior, Elevation gradient, Andes, Páramo transition zone, Andean shrubland, Microclimate, Integrated fire management

Resumen

Antecedentes Los incendios forestales constituyen una perturbación ecológica cada vez más importante en los ecosistemas andinos, en particular en matorrales de alta montaña y zonas de transición hacia el páramo. En el sur de Ecuador, el reciente aumento de la actividad de incendios subraya la necesidad de comprender cómo el comportamiento del fuego responde a fuertes gradientes altitudinales, donde las características del combustible, el microclima y la topografía cambian en distancias cortas. Este estudio examinó el comportamiento del fuego durante quemas prescritas en tres zonas altitudinales contrastantes (1549—2757 m s.n.m.) para identificar los principales controles

*Correspondence:
Angel Balaguer-Beser
abalague@mat.upv.es
Full list of author information is available at the end of the article

ecológicos y ambientales sobre la velocidad de propagación, la longitud de llama, la altura de llama y la temperatura del suelo a una profundidad de 5 cm.

Resultados El comportamiento del fuego varió sistemáticamente a lo largo del gradiente altitudinal, reflejando cambios en las restricciones ecológicas dominantes sobre la combustión. En las zonas de mayor altitud y pendiente pronunciada, la exposición al viento y las interacciones entre viento–pendiente favorecieron una propagación más rápida y un mayor desarrollo de las llamas. En las altitudes intermedias con pendientes moderadas, la humedad de la vegetación limitó la propagación y el desarrollo de las llamas, lo que indica que el estado hídrico de los combustibles vivos regula fuertemente la inflamabilidad incluso con un forzamiento atmosférico moderado. A menores elevaciones, con matorrales de suave pendiente, una mayor radiación solar y una mayor sequedad superficial se asociaron con un comportamiento del fuego más variable, en consonancia con la estructura de combustible fragmentada y una continuidad heterogénea. Estos patrones indican que el gradiente altitudinal no solo escala la intensidad del fuego, sino que reorganiza el equilibrio entre el forzamiento topográfico, las condiciones atmosféricas y las propiedades del combustible.

Conclusiones El comportamiento del fuego en paisajes andinos se rige por controles ecológicos que cambian con la altitud, en lugar de por un único factor dominante. Reconocer estos mecanismos específicos de cada zona puede fortalecer el Manejo Integrado del Fuego al alinear las estrategias de prevención, monitoreo y reducción de riesgos con el contexto ecológico de cada zona altitudinal.

Background

Fire weather conditions play a critical role in shaping fire behavior and determining the extent of burned areas (Bridge et al. 2005). Variations in these conditions influence the magnitude of ecological impacts, including vegetation mortality, post-fire regeneration, carbon emissions, soil heating, and hydrological responses (Keeley 2009; Robinne and Secretariat 2021). Fire behavior results from complex interactions among fuels, weather, and topography, which together regulate fire spread, flame characteristics, fire-line intensity, and heat transfer to the soil (Mhawej et al. 2015; Flannigan and Wotton 2001; Pausas and Keeley 2021).

In the tropical Andes of southern Ecuador, steep elevation gradients generate abrupt environmental transitions over short spatial distances. Temperature, humidity, vegetation structure, and fuel characteristics change rapidly along these gradients, creating substantial variability in fire behavior. Lower-elevation inter-Andean valleys are typically characterized by woody and shrub-dominated vegetation, whereas higher elevations support grasslands and páramo-like ecosystems, dominated by fine herbaceous fuels under cooler and more humid conditions. These transitions influence fuel structure, fuel moisture dynamics, and wind exposure, all of which strongly modulate fire intensity, rate of spread, and fire residence time (Ganteaume et al. 2013; Pausas and Keeley 2021). High-Andean ecosystems are increasingly influenced by anthropogenic disturbances, particularly cattle grazing, vegetation removal, and the use of fire for pasture management (Hofstede 1995; Kala 2023). These activities not only increase the probability of ignition but also modify fuel loads and spatial continuity. Frequent grazing promotes the dominance of fine, fast-curing fuels that facilitate rapid surface fire spread (Kerns et al. 2011), whereas shrub encroachment and vegetation thickening enhance vertical fuel continuity, increasing flame length, fire-line intensity, and soil heat transfer (Armenteras et al. 2013; Carrión-Paladines et al. 2022). Consequently, fire interacts with land-use pressures to accelerate ecosystem degradation by altering combustion patterns and fire severity.

These socio-ecological dynamics are clearly reflected across the study area. In San Lucas, livestock production dominates landscapes, which are composed primarily of grazed grasslands where recurrent burning is used to maintain pasture productivity (Coronel-Alulima 2019). These systems tend to accumulate fine, highly flammable fuels that dry rapidly during seasonal droughts, favoring fast rates of fire spread. In contrast, Malacatos represents shrub-dominated Andean landscapes with mixed agricultural activities, where higher aboveground biomass and vertical fuel continuity may support greater flame development and soil heating during burning (Armenteras et al. 2013; Carrión-Paladines et al. 2022). The landscapes in Loja add an additional dimension, as agricultural fires frequently occur near infrastructure and urban expansion zones, highlighting how human-modified fuel mosaics can generate fire behavior that increases risk at the wildland-urban interface (González et al. 2024). Moreover, it is necessary to study the behavior of fire in shrublands in all these areas because they are present throughout the elevation gradient.

Fire behavior emerges from the interaction of fuels, weather, and topography (Flannigan and Wotton 2001; Kala 2023). Fuel moisture regulates combustibility, with drier fuels igniting more readily and sustaining higher fire intensity. Vegetation structure and fuel continuity influence flame development and heat transfer. Weather conditions—particularly air temperature and wind speed—control fuel drying and oxygen supply, while wind direction determines fire-propagation pathways and spotting potential (Nelson 2002; Carrión-Paladines et al. 2022). Topography, especially slope, affects fire spread by enhancing convective and radiant heat transfer upslope. These controls vary substantially across elevation gradients in the Andes, where rapid environmental transitions can lead to strong contrasts in fire behavior over relatively short distances (Román-Cuesta et al. 2014; Zapata-Ríos et al. 2021).

Despite the ecological and social importance of elevation-driven variation in Andean fire regimes, experimental evidence directly linking environmental gradients to field-measured fire behavior remains scarce (Lippok et al. 2013). Experimental burns provide a valuable approach for quantifying fire behavior under controlled yet realistic field conditions, allowing direct measurement of fire spread, flame characteristics, and near-surface soil heating (Gimeno-García et al. 2004). However, few studies have examined fire behavior across elevation gradients in tropical mountain regions (Haire and McGarigal 2009), representing a key knowledge gap in fire ecology. The main objective of this study was to evaluate how climatic and topographic conditions, together with vegetation cover, influence fire behavior during controlled burns along an elevation gradient (1552–2754 m a.s.l.) in Andean ecosystems of southern Ecuador. Specifically, we asked how climatic conditions, topographic factors, and vegetation cover influence the rate of spread, flame length, and flame height along the elevation gradient. As a complementary response variable, we also evaluated near-surface thermal impact using soil temperature at a depth of 5 cm. We hypothesized that fire behavior and near-surface soil heating vary systematically along the elevation gradient as elevation reshapes microclimate, topographic exposure, and fuel-bed/vegetation condition (cover and moisture status) as proxied by spectral indices.

Consistent with this hypothesis, we expected that (i) at higher elevations with steeper slopes, topographic forcing and wind exposure would exert stronger control, resulting in faster spread rates and greater flame development; (ii) at mid elevations with moderate slopes, vegetation-moisture status (as indicated by spectral moisture indices) would emerge as a primary limiting factor, constraining fire behavior even under favorable atmospheric conditions; and (iii) at lower elevations with gentler slopes, higher solar exposure and surface drying would increase among-plot variability in fire behavior and soil heating due to heterogeneous fuel continuity and fuel mosaics. By clarifying how fire behavior responds to interacting environmental and land-use contexts, this study aims to improve understanding of wildfire impacts in Andean socio-ecological systems and to support the development of more effective integrated fire-management and risk-reduction strategies in southern Ecuador.

Materials and methods

Study area

The study area is located in Loja canton, southern Ecuador (Fig. 1). Experimental plots were located across an elevational gradient of 1549–2757 m a.s.l., where elevation-driven climate variability and complex topography generate sharp contrasts in air temperature, humidity, and fuel structure that can influence fire behavior. Across this mountainous landscape, four climatic belts are commonly recognized (cold, temperate, subtropical, and tropical), with the temperate belt occupying the largest area (Paladines 2013). The variation among climate types is fundamentally driven by the elevational gradient. Mean annual temperature ranges from 15.3 °C in Andean valleys to 7.3 °C at higher elevations (Ochoa-Cueva et al. 2015), while annual precipitation varies from 500 to 2000 mm (Municipio de Loja 2014). Air temperature decreases with altitude, while precipitation patterns, humidity, cloud formation, and radiation balance change due to orographic effects and atmospheric pressure gradients. The dry season extends from April to November and coincides with the highest wildfire occurrence (Carrión-Paladines et al. 2022), whereas the wet season occurs from November to April, with the highest monthly precipitation (Rollenbeck and Bendix 2011; Oñate-Valdivieso et al. 2018). During the rainy season, numerous high-intensity precipitation events occur due to storms passing over the inter-Andean valleys (Ochoa-Cueva et al. 2015). Notably, rainfall in the Ecuadorian Andes exhibits marked interannual variability, which can alter the onset, duration, and intensity of the wettest and driest phases, thereby modulating fuel moisture and influencing the occurrence of wildfires (Celleri et al. 2007; Carrión-Paladines et al. 2022).

To evaluate fire-behavior along an elevational gradient in Loja canton, southern Ecuador, three contrasting study zones were selected in the parishes of Malacatos (lower elevation), Punzara (mid elevation, peri-urban), and San Lucas (higher elevation) (Fig. 1). Key physiographic attributes and mean meteorological conditions during the burn period are summarized in Additional file 1: Table S1. Plots in San Lucas were located at the highest elevations (2752–2757 m a.s.l.) and on the steepest slopes (22–39°). Plots in Punzara were situated at intermediate elevations (2270–2278 m a.s.l.) with moderate slopes (14–21°), whereas plots in Malacatos occupied the lowest

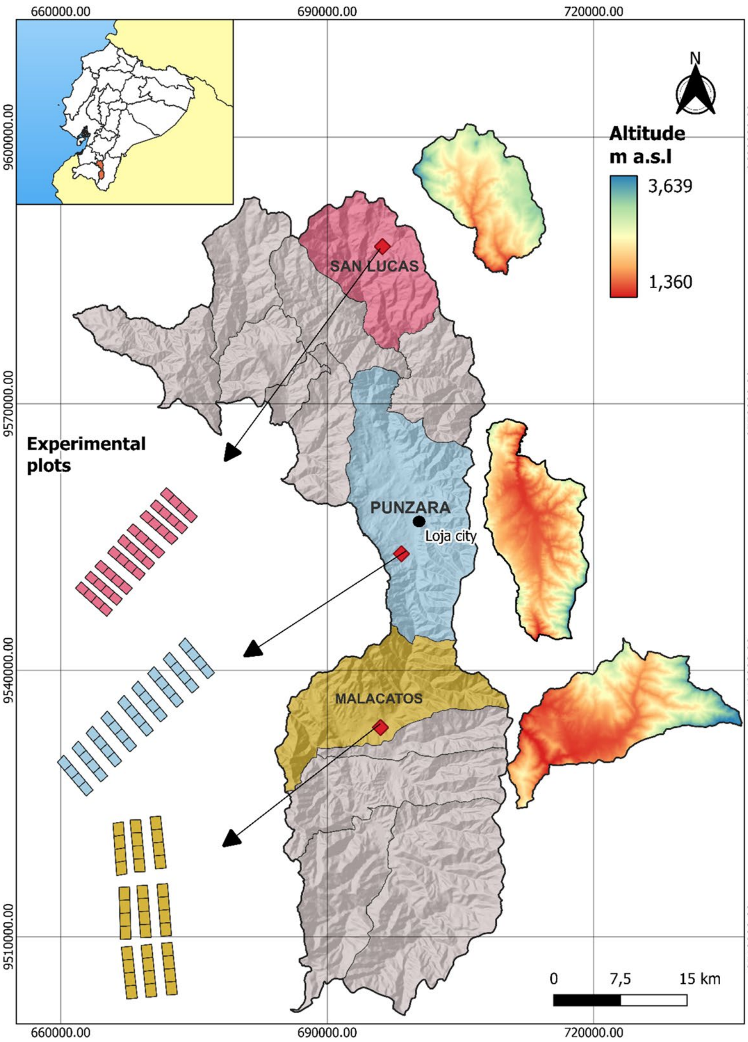

Fig. 1 Study zones along an elevational gradient in Loja canton, southern Ecuador. The map shows the parishes of San Lucas (higher elevation), Punzara (mid elevation; peri-urban), and Malacatos (lower elevation), where the three study zones were established. Arrows indicate approximate locations of the experimental plots; plot layouts are schematic and not to scale. Coordinate system: WGS84 / UTM Zone 17S

elevations (1549–1557 m a.s.l.) and the gentlest slopes (1.81–6.93°). For clarity, these values refer to plot-level ranges within each zone; zone-level means are reported in Additional file 1: Table S1. Although each zone spans an internal elevational range, the three zones differ not only in altitude but also in vegetation structure, land use, and fuel characteristics. Selecting distinct zones allowed us to capture socio-ecological and fuel-structure contrasts that would not be represented by a single continuous elevational transect within one locality.

Vegetation in the study zones differed in structure and species composition. In Malacatos, the herbaceous layer was dominated by species such as *Plantago australis*, *Ludwigia peruviana*, and *Cuphea racemosa*. In Punzara, representative species included *Tibouchina laxa*, *Desmodium tortuosum*, and *Cuphea racemosa*. In San Lucas, shrub-dominated vegetation included *Baccharis genistelloides*, *Gynoxys buxifolia*, and *Gaultheria erecta*. Predominant soils across the studied ecosystems are classified as Entisols and Inceptisols (Municipio de Loja 2014; IUSS Working Group WRB 2015).

Experimental design

Fire behavior was characterized following the experimental plot methodology proposed by Carrión-Paladines et al. 2023 for the herbaceous páramo of southern Ecuador. In each study zone (Malacatos, Punzara, and San Lucas), we established nine plots (4 m × 20 m) arranged as three randomized complete blocks (three plots per block; schematic in Fig. 2) to account for fine-scale topographic

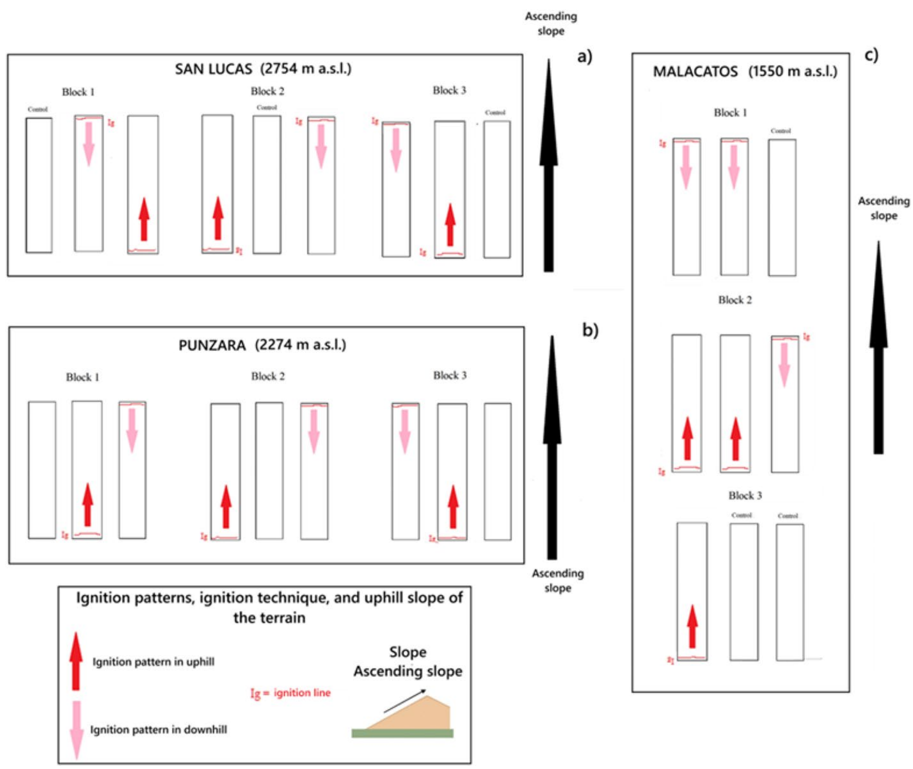

Fig. 2 Experimental setup using a Randomized Complete Block Design (RCBD) for controlled burning across an elevational gradient in Loja, Ecuador. The study includes three zones: (**a**) San Lucas (higher elevation), (**b**) Punzara (mid elevation), and (**c**) Malacatos (lower elevation). Each zone contains three blocks with randomly assigned treatments: upslope ignition, downslope ignition, and control. Plots are separated by a 3 m buffer to ensure independence. The ignition line (Ig) was established 30 cm from the inner plot edge

heterogeneity. Plot orientation varied by zone due to terrain constraints: northwest-facing in San Lucas and Punzara, and north-facing in Malacatos (Fig. 1). Within each block, the three fire treatments—upslope ignition, downslope ignition (with the slope), and an unburned control—were randomly assigned, following a randomized complete block design (RCBD). In San Lucas and Punzara, the comparatively steep slopes at the plot level (San Lucas: 22–39°; Punzara: 14–21°) required aligning blocks parallel to contour lines to ensure operational safety and maintain within-block topographic comparability. In Malacatos, the gentler slopes (1.81–6.93°) allowed a near-horizontal block layout, which minimized edge effects while preserving treatment independence. All blocks across all zones contained the full set of three treatments; the apparent asymmetry in Fig. 2c (Malacatos) reflects schematic labeling/layout conventions (e.g., the control shown at the lower end of the slope for clarity), not missing plots. The ascending-slope arrow in Fig. 2 is consistent across panels and always indicates the direction of increasing elevation (upslope), irrespective of plot orientation. To assess topographic controls on fire behavior, two slope-aligned burning patterns were applied (Fig. 2): downslope spread (with-slope) and upslope spread (against-slope).

In both burning patterns, ignition followed a strip-head technique (Waldrop and Goodrick 2012), with the ignition line (Ig) placed 0.30 m inside the plot boundary to reduce escape risk. Fires were lit using a 5-L drip torch charged with a 75:25 diesel–gasoline mixture. Plots were separated by 3-m buffer strips to minimize unintended fire spread, fenced with wooden posts and barbed wire to exclude cattle (Bos taurus), and burned under existing fuel loads (i.e., no fuel was added), consistent with natural grassland conditions (Hueso-González et al. 2018). Buffer strips were prepared by reducing fine-fuel continuity locally, rather than fully clearing vegetation: dry grasses, shrub material, and litter were selectively removed while low-flammability vegetation was retained.

Meteorological conditions were monitored in situ. Fire-weather variables were measured immediately before ignition and during each burn using a portable weather meter (Kestrel 5500, Nielsen-Kellerman, USA; accuracy: ± 0.5 °C for temperature, ± 2% for relative humidity, and ± 3% for wind speed) (Muñoz-Rojas et al. 2016) mounted at a height of 2 m at the plot center.

Recorded variables included air temperature (°C), relative humidity (%), wind speed (m s⁻1), and wind direction (° from north). Incoming solar radiation (W m⁻2) was measured concurrently using a portable pyranometer (Apogee SP-110, USA; accuracy: ± 5%). Experimental burns were conducted during the dry season (October–November 2024), which is typically characterized by dry and sunny conditions in the study region (Gutiérrez-Rodríguez et al. 2023). Burns were conducted between 09:00 and 15:00, when incoming solar radiation and air temperature are generally near their daily maxima and relative humidity near its minimum (Geron and Hays 2013). Fire-behavior response variables were flame height, flame length, and fire rate of spread. Within each plot (4 m × 20 m), flame metrics were referenced to four metal rods installed along the plot axis and spaced 5 m apart (Carrión-Paladines et al. 2023).

These rods, coated with fire-resistant paint and marked at 5-cm intervals, allowed flame height to be determined across different sections. Photographs were taken to corroborate visual estimates, and the images were coded and analyzed using UTHSCSA-ImageTool 3.0 (University of Texas Health Science Center at San Antonio, Texas, USA) (Brooks and Jack 2018) to obtain an average flame height per plot. Average flame height was used because maximum values tended to represent atypical or extreme conditions that were not representative of the overall fire behavior. Flame length, defined as the distance along the curvature of the flame, was visually estimated during the passage of the fire front in each experimental plot using the same metal rods employed for flame height measurement (Sullivan 2009; Rossa et al. 2024). Flame length was measured in meters, consistent with flame height, which also uses meters as the unit of measurement.

The fire rate of spread (R, m s^{-1}) was calculated as the linear distance travelled by the fire front per unit time between consecutive stations spaced 5 m apart, $R = d \bullet t^{-1}$, where d is distance (m) and t is the elapsed time (s) between front arrival at successive stations. Within each 4 m × 20 m plot, timing was recorded for four consecutive 5 m segments (0–5, 5–10, 10–15, and 15–20 m) along the central measurement axis, using four metal rods and the plot ends as reference stations, yielding segment-level estimates of R. Segment-level R values were averaged to obtain a plot-level estimate (Carrión-Paladines et al. 2023). In addition, soil temperature at a depth of 5 cm was recorded using three thermocouples per plot connected to EasyLog EL-USB-TC data loggers with K-type probes, installed along the central axis and aligned with the station positions (Rocha et al. 2019; Carrión-Paladines et al. 2023).

For the spectral characterization of vegetation cover, vegetation water status, and bare-soil exposure, we computed a suite of spectral indices derived from Sentinel-2 Level-2A surface reflectance imagery (see Additional file 1: Table S2) within the Google Earth Engine environment. These indices provide complementary information on canopy greenness and vegetation condition, moisture stress, and soil background, supporting a consistent description of pre-burn fuel status across the study area and capturing variability potentially associated with drought and other recent disturbances. We selected a cloud-free Sentinel-2 scene acquired approximately 2 months prior to the burn campaign to minimize cloud contamination while maintaining temporal proximity to the burn period. For each experimental plot location, index values were extracted from pixels overlapping the plot footprint and immediate vicinity and summarized as the mean, reducing pixel-level noise and providing stable plot-scale covariates for subsequent fire-behavior modeling and impact assessment; given the 10–20 m spatial resolution of Sentinel-2 bands, these values represent local conditions in the plot vicinity rather than within-plot heterogeneity.

The Normalized Difference Vegetation Index (NDVI) was used as a general indicator of vegetation greenness and photosynthetic capacity/vigor (Farbo et al. 2024), whereas the Green Normalized Difference Vegetation Index (GNDVI) provided increased sensitivity to chlorophyll-related variation and potential early stress signals (Mangewa et al. 2022). The Atmospherically Resistant Vegetation Index (ARVI) was also computed to estimate vegetation greenness while reducing the influence of atmospheric scattering (e.g., haze and aerosols) on reflectance-based metrics (Hakim et al. 2024). To limit soil-background effects under sparse canopy cover, the Soil-Adjusted Vegetation Index (SAVI) was calculated using its soil-adjustment factor (Huete 1988; Ren et al. 2018). Finally, the Bare Soil Index (BSI) was used to characterize bare-soil exposure and sparsely vegetated surfaces, supporting the assessment of surface exposure conditions in the plot vicinity (Ebrahimi et al. 2024).

For moisture analysis, three indices were calculated. The Normalized Difference Moisture Index (NDMI) and the Moisture Stress Index (MSI) were used to detect water availability in vegetation and levels of water stress, through a combination of near-infrared (NIR) and shortwave infrared (SWIR) bands (Lastovicka et al. 2020). The index called Moisture exploits the sensitivity of SWIR reflectance to leaf water content, while NIR reflects vegetation structure and vigor. Low values of the Moisture index indicated high water content and healthy vegetation, whereas high values indicated water stress, drought conditions, or dry surfaces (Liu et al. 2021). All indices were calculated from satellite imagery such as Sentinel-2 processed in Google Earth Engine environment, ensuring spatial and temporal standardization of the data for subsequent statistical and geospatial analyses (Fernández-Manso et al. 2016).

For the topographic variables, a digital elevation model (DEM) was generated from Drone Mavic 3 M imagery using photogrammetry, where overlapping RGB images were processed to create a dense point cloud. The point cloud was then interpolated into a raster surface model with a spatial resolution of 2 cm, providing elevation and slope data of the terrain (DJI 2023). The total area survey was 6.032 ha (14.41 acres).

Statistical analysis

The methodology can be summarized in the following steps:

1. Exploratory analysis and hypothesis testing across study zones.

To identify multivariate patterns and reduce redundancy among predictors, Principal Component Analysis (PCA) was performed. Prior to analysis, all variables were standardized (zero mean and unit variance). Components were retained according to Jolliffe's modified Kaiser criterion (eigenvalues > 0.7) and by requiring cumulative explained variance > 80% (Jolliffe 2011; Cangelosi and Goriely 2007; Zhu et al. 2024). PCA was applied separately to (i) the spectral indices described above (see also Additional file 1: Table S2) and (ii) meteorological–topographic variables (air temperature, relative humidity, solar radiation, wind speed, wind direction, slope, and elevation). Wind direction (θ_{from},°) was treated as a circular variable and expressed using $sin\left(\theta_{from}\frac{\pi}{180}\right)$ to avoid discontinuities at 0/360°. For analyses requiring wind forcing aligned with the plot spread/ignition axis, wind-from direction was converted to wind-toward direction as $\theta_{toward} = \left(\theta_{from} + 180\right)mod360$, and an along-axis wind component was derived as:

$$\cos\left(\widehat{\overrightarrow{WD} - \overrightarrow{BP}}\right) \times \text{Wind Speed} = WS\ cos((\theta_{toward} - \phi)\pi/180) \tag{1}$$

where WS is wind speed (m s^{-1}) and ϕ is the azimuth (°) of the plot spread/ignition axis (burning pattern, $\overrightarrow{BP}$). Air temperature used in the statistical analyses was the mean of spot readings collected at the plot edge during flame-front progression (see meteorological measurements).

One-way analysis of variance (ANOVA) assessed for differences in the means of fire-behavior responses (fire rate of spread, flame length, flame height, and soil temperature values at a depth of 5 cm) among study zones (San Lucas, Punzara, and Malacatos). Normality and homoscedasticity were verified using Shapiro–Wilk and Levene's tests. Post hoc comparisons employed Fisher's Least Significant Difference (LSD), following standard applications in ecological data (Piepho 2004).

2. Global Generalized Linear Models (GLM) across the elevation gradient.

Gaussian GLMs (Dobson and Barnett 2018) were fitted for fire rate of spread, flame length, flame height, and soil temperature at a depth of 5 cm using pooled observations from the three study zones and including the study zone as a fixed effect to account for among-zone differences. Candidate predictors included the meteorological and topographic variables described above, along with spectral indices (see Additional file 1: Table S2), and categorical descriptors of ignition orientation and burning pattern. For models involving wind direction, wind direction was treated as a circular variable and was considered as $\cos(\widehat{\overrightarrow{WD} - \overrightarrow{BP}}) \times \text{Wind Speed}$ as described above in Eq. (1), which yielded a signed wind-speed term aligned with the burn axis. Flame length model also considered an Azimuth Factor (AF) multiplying the wind speed and the wind direction, which took the value "1" when the burning pattern was oriented southward and "-1" when it was oriented northward. Collinearity was assessed using the Variance Inflation Factor (VIF), with a threshold of VIF < 5 (Kim 2019). Model reduction was performed using bidirectional stepwise Akaike's Information Criterion (AIC), retaining the most parsimonious specification when $\Delta AIC \leq 2$ (Carstens et al. 2010). Furthermore, only statistically significant predictors (p-value < 0.05) were selected. Residuals were checked to verify distributional assumptions and to identify influential observations (influence diagnostics).

3. GLM for each study zone.

Analyses were conducted separately by study zone (San Lucas, Punzara, and Malacatos) to avoid confounding between-zone differences with within-zone burning-pattern effects. The predictor sets mainly focused on how wind patterns, together with other meteorological data and spectral indices, and burning pattern descriptors influenced fire spread, flame length, flame height, and soil temperature at a depth of 5 cm. In Punzara, models were restricted to the most homogeneous experimental blocks described in Fig. 2 to reduce within-zone variance. The interaction between burning pattern and wind speed or wind direction was considered, using the factor BP, which equaled 1 when the burning pattern was upslope and − 1 when it was downslope. The same procedures for collinearity, model selection, and diagnostics, as in the global GLM were applied.

A complementary analysis was developed to analyze the soil temperature at a depth of 5 cm (T) as a response metric and burning pattern as a categorical predictor to study in more detail the effect of the slope on the characterization of the thermal impact near the surface in more detail. Observations absent due to sampling design were not imputed because they were structurally missing (missing by design). Effect size was reported as the within-zone contrast $\Delta T = T_{\text{Upslope}} - T_{Downslope}$ so $\Delta T > 0$ indicated warmer soil under upslope burning. Because multiple observations were obtained within each plot, inference was made robust against within-plot dependence and potential heteroskedasticity: *p*-values for ΔT were computed using HC3 heteroskedasticity-robust standard errors (HC3 *p*-value), and 95% confidence intervals (95% CI) were obtained via a PlotID cluster-bootstrap percentile interval (resampling plots to preserve within-plot dependence). Influence was assessed using Cook's distance (threshold 4/n; n indicates non-missing observations). When influential observations were detected, ΔT was compared between the full fit and a sensitivity fit excluding those observations.

4. Additive modeling of nonlinear responses.

To capture potential nonlinear relationships, we used Generalized Additive Models (GAM) with Gaussian family and identity link (Wood 2011; Arcos et al. 2023). Smooth terms were fitted with penalized cubic regression splines, using conservative basis dimensions ($k \leq 4$) and smoothing parameter selection by REML. Shrinkage penalties (select = TRUE) were included to reduce overfitting and to allow the removal of negligible smooths. Effective degrees of freedom (edf) and approximate F-tests were reported for smooth terms and parametric coefficients were tested with t-statistics. In cases where GAMs produced non-significant smooths with very low edf, the simpler GLM was retained to preserve parsimony and interpretability.

5. Error metrics and reporting.

The adjusted coefficient of determination (Adj-R^2), percentage of variance explained by the model (Deviance) and Variance Inflation Factor (VIF), along with coefficient estimates and *p*-values indicating the level of statistical significance of model predictors are reported. Root Mean Square Error (RMSE) and Mean Absolute Error (MAE) were expressed as percentages relative to the range observed in the response variable using Eq. (2),

$$RMSE\% = 100\frac{\sqrt{\frac{1}{N}\sum_{i=1}^{N}\left(y_i - \widehat{y}_i\right)^2}}{ymax - ymin},$$
$$MAE\% = 100\frac{\frac{1}{N}\sum_{i=1}^{N}\left|y_i - \widehat{y}_i\right|}{ymax - ymin} \qquad (2)$$

where y_i is the observed value, $\hat{y}_i$ is the model prediction, ymax is the maximum and ymin is the minimum of observed values for the corresponding dataset. Thresholds for statistical significance were set at $\alpha = 0.05$, with $p < 0.10$ reported as marginally significant when ecologically justified.

All analyses were performed in R (v4.x) using the following packages: stats (base modeling), car (collinearity and ANOVA), mgcv (GAM fitting), FactoMineR and factoextra (PCA), performance (diagnostics), ggplot2 (graphics), and agricolae (LSD tests). Some scatter plots, box and whisker plots, and graphs from ANOVA and PCA were also obtained with Statgraphics Centurion (The Plains, Virginia, USA).

Results

Physiographic characterization and differential analysis of fire behavior between study zones

Five main components with eigenvalues greater than 0.7 were retained when considering the set of meteorological and topographic variables, which explained 82.78% of the total variance. Principal Component 1 (PC1) explained 31.82% of the total variance (eigenvalue of 2.86) and was characterized by strong positive loadings for Slope (0.564) and Altitude (0.561), and substantial negative loadings for Temperature (− 0.464) and Solar Radiation (− 0.239). This component represented a topographic–thermal gradient, whereby higher elevation and steeper terrain were associated with lower temperatures and reduced incoming solar radiation. PC2 accounted for 19.88% of the variance and was defined by a strong negative loading for Relative Humidity (− 0.544) and Solar Radiation (− 0.339), together with significant positive loadings for Wind Speed (0.462) and the Sine of Wind Direction (0.438). These variables contributed to a lesser extent to the separation of the data (see Additional file 1: Fig. S1). PC3 contributed 11.87% of the total variance and was overwhelmingly dominated by the $\cos(\widehat{\overrightarrow{WD} - \overrightarrow{BP}}) \times \text{Wind Speed}$ variable, which exhibited a remarkably high loading (0.850). PC4 and PC5 explained, respectively, 10.96% and 8.26% of the total variance.

Spectral variables indicated differences in vegetation between study zones. Variables related to photosynthetic activity, such as ARVI and GNDVI, showed differences between the three zones, with Punzara being particularly distinct (see Additional file 1: Fig. S2). Other variables related to vegetation moisture content, such as NDMI, showed smaller values in higher-altitude locations (San Lucas). The first two principal components calculated with spectral variables explained 96.5% of the total variability. NDMI, MSI, Moisture, and BSI had significant weight in the first principal component (PC1_spectral), which separated the data from the Malacatos and San Lucas study zones. A high value in PC1_spectral indicates little presence of bare soil and low water stress. Meanwhile, GNDVI, SAVI, NDVI, and ARVI had significant weight in the second principal component (PC2_spectral) differentiating the data collected from Punzara (see Additional file 1: Fig. S2). PC2_spectral is the indicator of growth and phenological state, so plots with high PC2_spectral values were those with very active and vigorous vegetation. These groupings of spectral variables were taken into account in the final selection procedure of predictors for the models developed in this results section.

An analysis of variance (ANOVA) showed that there was a statistically significant difference between the averages of the Malacatos and San Lucas study zones in the fire rate of spread and the flame height (Fig. 3). Moreover, the Punzara study zone showed lower soil temperature values at a depth of 5 cm (Fig. 3).

Drivers of fire behavior across the elevational gradient

GLM models for four dependent variables based on data from the entire elevation gradient are shown in Table 1. These models allowed for the identification of general patterns in fire dynamics, but they showed limited explanatory capacity, with Adj-R^2 values of 44.7% for fire rate of spread, 32.6% for flame length, 22.1% for flame height and, 44.02% for soil temperature at a depth of 5 cm, highlighting the predominant influence of local and zone-specific factors. In contrast, RMSE% and MAE% showed errors between 10.15% and 17.39%.

Table 1 only shows statistically significant predictors (p value < 0.05) after the stepwise selection procedure.

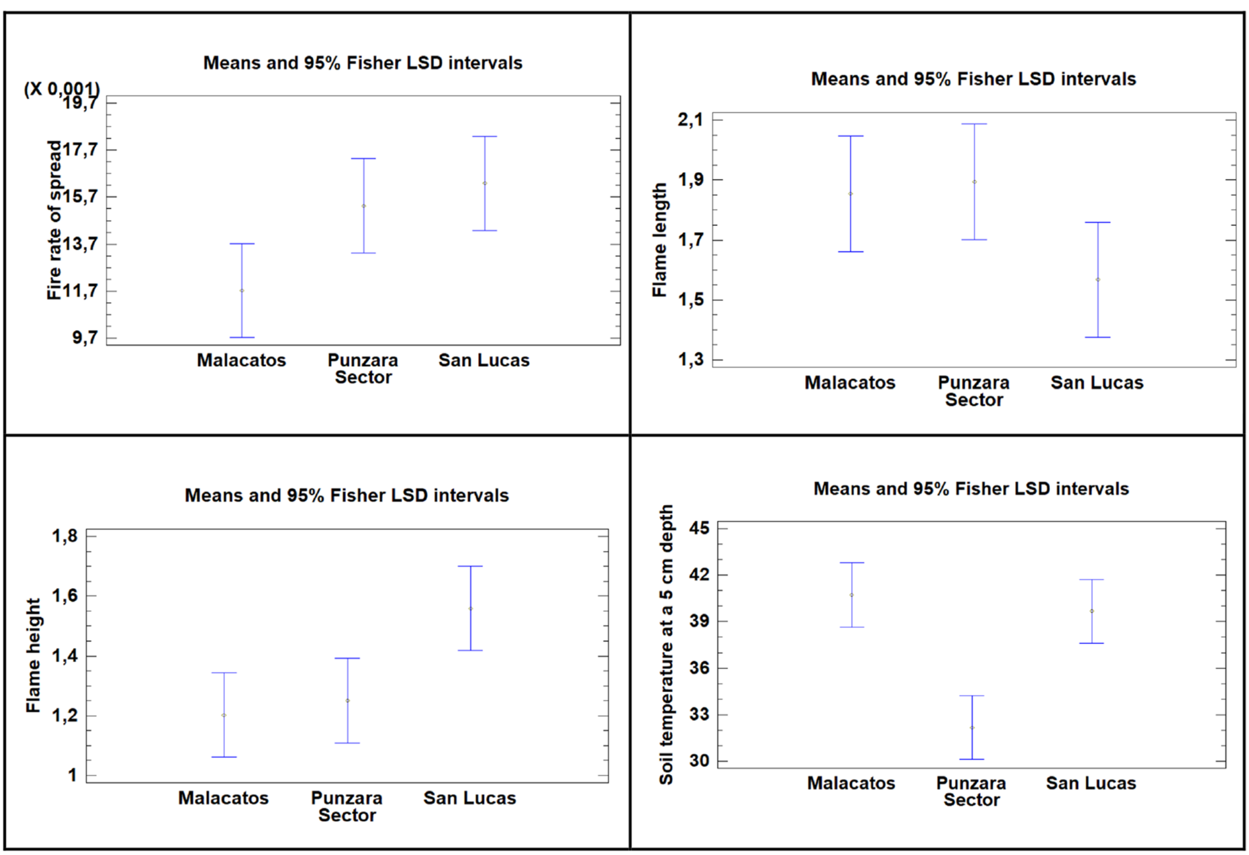

Fig. 3 Results using Fisher's Least Significant difference (LSD) procedure in the Analysis of Variance to analyze the difference among the means of each study zone

Table 1 Coefficients (Coef.) and statistics of the GLM for fire rate of spread, flame length, and flame height applied to the entire elevation gradient in Loja, southern Ecuador. The burning pattern (Burn. pattern) was coded categorically: 1 when burning was upslope and, − 1 when downslope. The term, $\cos(\widehat{\overrightarrow{WD} - \overrightarrow{BP}}) \times \text{wind speed}$, was computed using Eq. (1). AF (Azimuth Factor) is an index that takes the value "1" if the burning pattern is towards the south and "− 1" if the burning pattern is towards the north. Root Mean Square Error (RMSE%) and Mean Absolute Error (MAE%) were expressed as percentages relative to the range observed in the response variable (see Eq. (2))

Study zone	Dependent variable	Formula	*Coef*	*p*-value	Adj-R^2 (%)	RMSE%	MAE%	VIF
All data	Fire rate of spread (m s^{-1})	Intercept	− 0.01782	-	44.70%	13.45%	10.26%	-
		Burn. pattern	0.002208	0.004				1.38
		$\cos(\widehat{\overrightarrow{WD} - \overrightarrow{BP}})$×wind speed	0.001206	< 0.001				1.05
		Temperature	0.000703	0.021				2.26
		Altitude	0.000006	0.002				1.92
All data	Flame length (m)	Intercept	1.99726	-	32.60%	17.39%	12.91%	-
		ARVI	2.24289	0.003				1.00
		AFxWind speed	0.203128	0.038				2.76
		AFxWind direct	− 0.00254	0.026				2.76
All data	Flame height (m)	Intercept	− 0.26862	-	22.07%	14.99%	10.15%	-
		Wind speed	0.226339	< 0.001				1.14
		Rel. humidity	0.018737	0.005				1.17
		Wind direction	0.001866	0.030				1.02
All data	Soil temperature at a depth of 5 cm	Intercept	27.9328	-	44.02%	16.37%	12.57%	-
		Burn. pattern	2.69598	< 0.001				1.00
		NDVI	42.1216	< 0.001				1.00

The coefficients have been ordered so that the constant appears first, the categorical factor appears second, followed by the remaining factors in decreasing order of the coefficients. The selected variables for fire rate of spread were the burning pattern, air temperature, altitude, and $\cos(\widehat{\overrightarrow{WD} - \overrightarrow{BP}}) \times$ wind speed. The most relevant effects for flame length corresponded to the terms AF × wind direction and AF × wind speed, along with the ARVI spectral index associated with vegetation cover and condition. The recorded wind direction values for these plots ranged from 0 to 234°, indicating the azimuth angle relative to geographic north. For flame height, the variable most strongly associated was wind speed, followed by wind direction and relative humidity, which directly influenced the vertical development of the flames. Soil temperature at a depth of 5 cm was modeled using the burning pattern and the NDVI spectral index.

The Adj-R^2 values obtained indicate that, although some predictors showed relevant effects at the general scale (such as temperature, altitude, or burning pattern), fire spread, vertical development, and horizontal extension processes were primarily influenced by more specific spatial factors. Therefore, a stratified analysis by study zones was conducted, as detailed in the following sections.

How fire behavior responds to local conditions in each ecosystem type

In San Lucas, the rate of fire spread was strongly explained by the burning pattern and ambient temperature (Table 2), such that changes in the burning pattern significantly increased the rate of fire spread, and higher temperatures resulted in a faster rate of spread. This model yielded a high Adj-R^2 of 73.5% with relatively low errors (RMSE% = 13.45%). Flame length was primarily explained by the burning pattern, wind speed, and relative humidity, although the adjustment in this case was more moderate (Adj-R^2 = 57.51%) Flame height was positively associated with wind speed and direction, with wind speeds ranging from 0.9 to 2.7 m s^{-1} and prevailing wind directions between 99° and 148.5°. A linear combination of three spectral indices also influenced flame height, with ARVI and GNDVI having negative effects, while NDMI made a moderate positive contribution. There was strong multicollinearity among the vegetation indices, and the individual coefficients should be interpreted with caution, but this model was presented to show that flame height is well explained by wind and vegetation structure/state (Adj-R^2 = 71.58%). Finally, the burning pattern significantly increased the soil temperature at a depth of 5 cm, although the Adj-R^2 is low (26.40%) and the errors were high.

Accurate results were only obtained in Punzara with the GLM applied to the plots of the first two blocks (see description of blocks in Fig. 2). In Block 3, vegetation was less homogeneous, with lower NDVI values than in the other blocks (the difference was statistically significant in the ANOVA test). Model performance was satisfactory, with Adj-R^2 values ranging from 55.7% to 79.3%, relatively low prediction errors (RMSE% and MAE% < 20%),

Table 2 Continuation of Table 1, but with specific GLM results for the study zones of San Lucas, Punzara and Malacatos. BP equals 1 when the burning pattern was upslope and − 1 when downslope. Description of blocks in Punzara are given Fig. 2. Sin (W. dir) is the sinus of the wind direction

Study zone	Dependent variable (units)	Formula	*Coef*	*p*-value	Adj-R^2%	RMSE%	MAE%	VIF
San Lucas	Fire rate of spread ($m\ s^{-1}$)	Intercept Burn. pattern Temperature	− 0.020669 0.0062025 0.001385	- < 0.001 0.002	73.46%	13.48%	10.58%	- 1.17 1.17
San Lucas	Flame length (m)	Intercept Burn. pattern Wind speed Rel. humidity	− 1.55682 0.327569 0.362063 0.0477047	- 0.001 < 0.001 0.005	57.51%	14.47%	9.22%	- 1.56 1.19 1.28
San Lucas	Flame height (m)	Intercept Wind speed Wind direction ARVI GNDVI NDMI	1.96661 0.296067 0.0039867 − 127.375 − 64.3025 130.862	- < 0.001 0.012 < 0.001 < 0.001 < 0.001	71.58%	11.81%	8.65%	- 1.02 1.54 30.69 5.39 41.36
San Lucas	Soil temp. at depth of 5 cm (°C)	Intercept Burn. pattern	39.6722 2.62778	- 0.017	26.40%	19.56%	14.24%	- 1.0
Punzara Block < 3	Fire rate of spread ($m\ s^{-1}$)	Intercept BPxWind sp. NDMI	0.01978 0.00093 − 0.1711	- 0.007 0.012	65.46%	13.48%	13.07%	- 1.17 1.17
Punzara Block < 3	Flame length (m)	Intercept BPxWind dir BPxWind sp.	2.04739 0.00854 − 0.5481	- 0.007 < 0.001	55.74%	19.46%	11.89%	- 3.65 3.65
Punzara Block < 3	Flame height (m)	Intercept Wind speed BPxWind dir NDMI	0.82026 0.38978 0.00236 − 22.161	- 0.008 0.005 0.005	71.72%	13.70%	9.37%	- 1.00 1.04 1.04
Punzara Block < 3	Soil temp. at depth of 5 cm (°C)	Intercept Burn. pattern Wind direct NDVI	− 3.5070 2.35199 0.0388 276.003	- 0.014 0.023 0.001	79.31%	13.13%	8.32%	- 1.16 1.22 1.06
Malacatos BP = 1	Fire rate of spread ($m\ s^{-1}$)	Intercept Radiation	− 0.08656 0.001399	- 0.002	58.66%	21.15%	16.59%	- 1.0
Malacatos BP = 1	Flame length (m)	Intercept Sin(W. dir) BSI	2.36643 − 0.58708 5.80946	- 0.003 0.002	74.59%	13.06%	9.44%	- 1.00 1.00
Malacatos BP = -1	Fire rate of spread ($m\ s^{-1}$)	Intercept Temp Radiation Wind dir NDMI	− 0.01225 0.002284 − 0.00063 0.000021 − 0.02582	- < 0.001 < 0.001 0.015 0.016	94.96%	8.30%	5.67%	- 1.60 1.22 1.27 1.41
Malacatos BP = -1	Flame height (m)	Intercept Rel. Humidity	0.071286 0.026007	- 0.017	38.86%	22.41%	16.32%	- 1.0
Malacatos	Soil temp. at depth of 5 cm (°C)	Intercept Moisture	34.7499 100.578	- 0.044	18.16%	21.16%	16.07%	- 1.0

and no evidence of problematic multicollinearity among predictors (VIF < 4) (Table 2), indicating moderate to high explanatory capacity under relatively uniform topographic conditions. Wind speed was selected as a predictor for flame height and the fire rate of spread model in Punzara (Block < 3). However, the sign of its contribution to the latter dependent variable depended on the burning pattern, being positive with an upslope fire and negative otherwise, indicating that under specific burn configurations, increasing wind speed substantially enhanced fire propagation. Flame length was explained by wind direction and wind speed, and both were modulated by the burning pattern. For flame height, the model incorporated direct effects of wind speed and an interaction between wind direction and burning pattern. Despite moderate RMSE% values (19.46%), the low MAE% (11.89%) indicated acceptable predictive stability. NDMI showed a strong negative effect on fire rate of spread and, especially on the flame height, suggesting that vegetation moisture content acted as a limiting factor for fire propagation and vertical flame development. The model for soil temperature exhibited the highest overall fit (Adj-R^2 = 79.31%). Burning pattern, wind direction, and NDVI showed a significant positive association with soil temperature. Low RMSE% (13.13%) and MAE% (8.32%) values further confirmed the robustness of this model.

In Malacatos, GLM performance varied markedly between burning patterns (Table 2), allowing explicit evaluation of contrasting fire–terrain configurations. The results revealed strong contrasts between upslope and downslope wildfire behavior. Fire rate of spread was significantly influenced by solar radiation, with higher irradiance values promoting faster propagation under an upslope ignition pattern. This relationship was captured by a simple univariate model (Adj-R^2 = 58.7%), consistent with the enhanced drying and preheating of fuels under high-radiation scenarios. The moderate prediction errors (RMSE% = 21.15%; MAE% = 16.59%) suggest acceptable but limited predictive accuracy. With a downslope burning pattern, a GLM including temperature (positive coefficient) and solar radiation (negative coefficient) accounted for 87.3% of the variation in fire rate of spread. NDMI values, indicative of vegetation water content, further improved the model when included, with more negative values (drier vegetation) correlating with faster spread. In this way, a GLM explaining almost 95.0% of the variation was computed, considering four predictors: temperature, radiation, wind direction, and NDMI (Table 2). Very low prediction errors (RMSE% = 8.30%; MAE% = 5.67%) reflect excellent model performance.

For flame length, the best-fit model in Malacatos (Adj-R^2 = 74.6%) included the bare soil index (BSI) as a positive predictor, but only in cases with an upslope burning pattern. The sine of wind direction had a significant negative effect, indicating that certain wind alignments related to slope reduce flame extension. Low RMSE% (13.06%) and MAE% (9.44%) indicate strong model reliability. However, no reliable model could be established for flame length under a downslope burning pattern. In contrast, a statistically valid model was identified under this last burning pattern for flame height, where such dependent variable was positively associated with relative humidity (Adj-R^2 = 36.6%) although the relatively high prediction errors (RMSE% = 22.41%; MAE% = 16.32%) indicated greater variability and reduced predictability of flame height in downslope wildfires. In the case of using soil temperature at a depth of 5 cm as a dependent variable, we only obtained a statistically significant model when pooling all burning patterns. However, that GLM exhibited low explanatory power (Adj-R^2 = 18.16%) and fuel moisture was the only significant predictor and showed a positive effect. The high RMSE% (21.16%) and MAE% (16.07%) indicated substantial unexplained variability.

Accounting for the nested sampling (multiple observations within PlotID) and using robust inference, we estimated the within-zone contrast between upslope and downslope burning for post-fire soil temperature at a depth of 5 cm (see Additional file 1: Table S3). In Malacatos, the estimated contrast was positive but highly uncertain ($\Delta T = 2.70$ °C; 95% CI= [−3.11, 8.51]) and did not provide evidence of a directional effect ($p = 0.408$). In contrast, upslope burning was associated with higher soil temperature at a depth of 5 cm than downslope burning in Punzara ($\Delta T = 6.56$ °C; 95% CI= [1.68, 11.43]; $p = 0.019$) and San Lucas ($\Delta T = 4.14$ °C; 95% CI= [2.02, 7.10]; $p = 0.029$). Overall, these results indicate that the soil thermal response to burning pattern differs among zones, while the observed contrasts are consistent with zone-specific controls (e.g., soil moisture, fuel-bed structure, and heating duration) that were not directly quantified here.

Nonlinear responses of fire behavior to environmental gradients

In the higher elevation study zone with steep slopes (San Lucas), GAMs exhibited the greatest predictive performance across the gradient, capturing the complexity of interactions among meteorology, topography, and fuels (Table 3). The fire rate of spread reached an Adj-R^2 of 85.6% and explained deviance of 91.0%, with the burning pattern as a highly significant predictor ($p < 0.001$) and maximum temperature as a relevant covariate ($p = 0.083$). Flame length achieved a similarly robust fit (Adj-R^2 = 82.2%, Deviance = 90.2%), driven by relative humidity ($p = 0.001$), wind speed ($p < 0.001$), and burning pattern ($p < 0.001$). For flame height, GAMs provided a moderate fit (Adj-R^2 = 46.2%, Deviance = 66.6%), with wind speed ($p = 0.038$) and burning pattern ($p = 0.016$) as significant predictors. Although less explanatory than fire rate of spread or flame length, this model confirms the dependence of vertical fire dynamics on wind flow and fire front orientation. Collectively, the San Lucas results demonstrate that GAMs are particularly effective at capturing nonlinear relationships in high-mountain ecosystems, where humidity gradients and topographic orientation strongly modulate fire behavior.

In the mid-elevation moderately steep study zone (Punzara), characterized by transitional conditions between humid shrubland and more open areas, GAMs showed variable performance (Table 3). The rate of spread was primarily explained by the NDMI (Adj-R^2 = 31.5%, Deviance = 39.9%, $p = 0.021$), highlighting the importance of vegetation water content as a controlling factor in fire spread across ecotones. By contrast, flame length

Table 3 Continuation of Tables 1 and 2, but with metrics of GAM (or applicable GLM) for fire behavior variables (fire rate of spread, flame length, flame height) across the study zones of San Lucas, Punzara, and Malacatos, Loja, southern Ecuador. Smooth terms were fitted with penalized cubic regression splines, using conservative basis dimensions ($k=4$)

Study zone	Model	Dependent variable (units)	Formula	*p*-value	edf	Adj-R^2 (%)	Deviance %	RMSE%	MAE%	VIF
Punzara	GAM	Fire rate of spread (m s^{-1})	s(NDMI)	0.021	2.809	31.5%	39.9%	19.14%	15.07%	1.35
	GAM	Flame length (m)	s(NDMI)	0.077	2.204	42.2%	56.8%	16.97%	13.62%	1.35
			s(Rel. humidity)	0.084	1.000					1.15
	GAM	Flame height (m)	s(NDMI)	0.022	1.000	57.3%	65.2%	13.14%	9.31%	1.35
			s(Wind speed)	0.004	2.284					1.30
San Lucas	GAM	Fire rate of spread (m s^{-1})	s(Max. temperat.)	0.083	2.310	85.6%	91.0%	7.70%	6.16%	2.41
			Burning pattern	< 0.01						1.24
	GAM	Flame length (m)	s(Rel. humidity)	0.001	2.126	82.2%	90.2%	6.81%	5.33%	2.27
			s(Wind speed)	< 0.001	1.000					1.09
			Burning pattern	< 0.001						1.24
	GAM	Flame height (m)	s(Wind speed)	0.038	1.900	46.2%	66.6%	12.53%	8.60%	1.09
			Burning pattern	0.016						1.24
Malaca_tos	GLM	Fire rate of spread (m s^{-1})	Burning pattern	0.082	-	33.1%	33.17%	21.83%	18.19%	1.44
			MSI	0.124	-					2.66
	GAM	Flame length (m)	Burning pattern	0.014	1.000	31.5%	49.6%	18.07%	14.15%	1.44
	GAM	Flame height (m)	s(Rel. humidity)	0.001	2.171	67.9%	79.2%	10.58%	8.64%	1.32

displayed very limited performance (Adj-R^2 = 42.2%, Deviance = 56.8%), with nonsignificant smooth terms for NDMI and relative humidity ($0.07 < p < 0.1$) and high error values (RMSE% = 17%, MAE% = 13.6%). Flame height, however, achieved a substantially stronger fit (Adj-R^2 = 57.3%, Deviance = 65.2%) with significant effects of NDMI ($p = 0.022$) and wind speed ($p = 0.004$).

In the lower elevation study zone with gentle slopes (Malacatos), GAM applied to the fire rate of spread was inadequate (Adj-R^2 = 9.2%, Deviance = 19.5%) with non-significant smooth predictors ($p > 0.1$). Given this poor performance, a GLM was retained, achieving a more stable fit (Adj-R^2 = 33.1%, Deviance = 33.17%) with interpretable linear predictors (burning pattern and radiation) (Table 3). This methodological decision was based on parsimony and statistical stability, avoiding the risk of overfitting often associated with GAMs when sample sizes are small ($n = 24$) and no strong nonlinear patterns are evident (Wood 2011). For flame length, GAMs showed a modest fit (Adj-R^2 = 31.5%, Deviance = 49.6%) with burning pattern as a significant predictor ($p = 0.014$). Flame height, in contrast, exhibited a strong fit (Adj-R^2 = 67.9%, Deviance = 79.2%) with relative humidity as the dominant predictor ($p = 0.001$).

Discussion

Elevation-dependent fire behavior patterns and control

Several studies have examined fire behavior at different altitudes (Bekker and Taylor 2001; Grau 2001; Argibay and Renison 2018; Argañaraz et al. 2020), although most research on fire ecology in the Andes has focused on the occurrence of fires, indigenous use of fire, impacts on vegetation, or factors that drive land use (Keating 2007; Román-Cuesta et al. 2014; Díaz et al. 2023). This study provides an empirical assessment of fire behavior, showing systematic variation along the Andean elevation gradient, indicating that elevation reorganizes the coupled system of microclimate, fuels, and flame dynamics rather than imposing a single dominant control across the landscape (Povak et al. 2018; Veblen 2008). The contrasts among higher-elevation San Lucas, mid-elevation Punzara, and lower-elevation Malacatos are consistent with "threshold" fire behavior, in which the relative importance of atmospheric conditions, fuel properties, and topographic exposure shifts once critical environmental conditions are crossed (Pausas and Keeley 2021). In mountainous terrain, such transitions are expected because topography and terrain-driven winds simultaneously modify the physical environment of spread and the ecological context in which combustion occurs (Povak et al. 2018; Storey et al. 2021).

Modeling results with GLMs integrating all observations confirmed that fire dynamics were primarily controlled by local interactions among wind, vegetation, and topography. Mechanistically, elevation reshapes air temperature, relative humidity, and wind exposure, drivers that influence fire behavior through two main pathways: (i) changes in live and fine-fuel moisture (Silva et al. 2022) and (ii) changes in fuel structure and continuity (Sullivan 2009; Pausas and Keeley 2021). In exposed, high-elevation settings such as San Lucas, steep slopes combined with greater wind exposure favor strong wind–slope coupling. This interaction enhances convective and radiative heat transfer, increases preheating of unburned fuels, and promotes faster upslope spread and flame development under dry conditions (Sullivan 2009; Storey et al. 2021; Cruz et al. 2022b). Our models developed for San Lucas indicated that in cold environments, fire spread responds strongly to thermal thresholds and the alignment of the upward-sloping ignition front. Relative humidity, wind speed, and burning pattern explained the lateral expansion of the fire front, which is consistent with experimental evidence in high-Andean páramo ecosystems where herbaceous vegetation promotes continuous flame fronts (Cruz et al. 2022a). Ecologically, these conditions suggest a higher potential for rapid fire growth and elevated soil heating, which can amplify impacts on belowground biota and slow post-fire recovery in high-Andean vegetation.

At mid elevations such as Punzara, where vegetation moisture and structural characteristics may impose stronger constraints on flammability, fire behavior appears more sensitive to short-term drying and fuel moisture dynamics. Our results emphasized the dominant role of wind (speed and direction) and spectral vegetation indices (NDMI and NDVI) in controlling fire behavior (Hao et al. 2022) and soil thermal response. In these systems, periods of reduced live and fine fuel moisture may temporarily relax these constraints, allowing fire spread and flame development to approach those observed under more wind-driven conditions. This indicates that fire activity at intermediate elevations may be more episodic, with pronounced responses to climatic variability and short-term weather anomalies (Pausas and Keeley 2021). Our analysis suggested that while spectral indices may partially explain lateral flame dynamics, other factors such as fine-scale fuel continuity likely play a role. These limitations were also reported in Mediterranean and Cerrado transitional ecosystems (Camprubí et al. 2022; Hakkenberg et al. 2024).

In contrast, lower-elevation systems such as Malacatos are strongly influenced by land-use legacies and landscape fragmentation, which can limit horizontal and vertical fuel continuity (Tapia-Armijos et al. 2015). Our models also indicated that atmospheric conditions, particularly relative humidity, appeared to exert greater influence on combustion efficiency, likely due to lower biomass loads and greater exposure to direct solar radiation. Under these conditions, fire spread may depend on the presence of fine, well-cured fuels and localized connectivity among fuel patches. As a result, similar meteorological forcing may translate into more spatially variable fire behavior, with alternating zones of active spread and self-limitation. Ecologically, this pattern implies a mosaic of fire effects, where some patches experience substantial biomass consumption and soil heating, while adjacent areas remain only lightly affected.

These patterns indicate that the Andean elevation gradient is associated with a shift from predominantly wind- and topography-driven fire behavior at higher elevations to more fuel-limited and connectivity-dependent fire dynamics at lower elevations. This altitudinal reorganization has important socio-ecological implications: it influences not only the potential rate of fire spread and flame development, but also the likelihood of severe soil heating, vegetation mortality, and post-fire recovery trajectories. Understanding how these controls vary with elevation is therefore essential for anticipating spatial differences in fire impacts and for designing management strategies adapted to the specific fire behavior regimes of high-Andean landscapes (Barros et al. 2018; Pausas and Keeley 2021).

Ecological processes underlying dominant controls of fire behavior

The results of this paper showed that wind speed and direction modulate the dimensions of the flame in areas of higher elevation and steeper slope. The recurrent importance of wind-related factors along the gradient is ecologically consistent with the fundamental role of airflow at the flame front. Wind enhances oxygen supply, tilts flames toward unburned fuel, and increases convective and radiative heat transfer, thereby accelerating fire spread and promoting vertical flame development (Sullivan 2009; Cruz et al. 2022b). In mountainous terrain, these processes are further shaped by slope-driven channeling and localized accelerations that create strong near-surface flow variability (Storey et al. 2021; Povak et al. 2018). Ecologically, this means that exposed upland systems are predisposed to rapid and spatially uneven fire spread, where small differences in terrain position can translate into large differences in fire intensity and flame structure (Storey et al. 2021; Veblen 2008).

Moisture-sensitive spectral indices such as NDMI can be interpreted as indicators of vegetation water status and, consequently, live-fuel moisture constraints on combustibility (Costa-Saura et al. 2021). Mid-elevation and mid-slope shrubland landscape models developed in this paper were characterized by the spectral variable NDMI together with interactions between burning pattern and wind speed or wind direction. Rather than representing a purely statistical relationship, the influence of NDMI reflects the ecological control exerted by plant water content on ignition and flame propagation. When live and fine fuels retain higher moisture, combustion is inhibited and fire spread remains limited; when moisture constraints relax during dry periods, flammability increases, and fires can respond more strongly to wind and topographic forcing (Yebra et al. 2013; Camprubí et al. 2022). This highlights how short-term climatic variability interacts with vegetation physiology to regulate when and where fires can transition from low-intensity surface spread to more active flame development.

Patterns of post-fire soil temperature further reinforce this ecological interpretation. Soil heating represents a key pathway through which fire behavior translates into ecosystem effects, influencing soil structure, nutrient cycling, microbial communities, and seed bank survival (Certini 2005; Santín and Doerr 2016). Because belowground heating depends on flame residence time, near-surface fuel consumption, and fine-scale heat transfer (Gimeno-García et al. 2004; Certini 2005), its spatial expression is inherently heterogeneous and sensitive to local fuel and terrain conditions. Differences between with-slope and against-slope burning therefore reflect not only directional fire spread, but also how combustion duration and heat transfer are modulated by vegetation structure and fuel continuity along the gradient. The stronger soil warming associated with with-slope burning in Punzara and San Lucas suggests that, in these zones, fuel structure and terrain conditions favor longer residence times and more sustained heat transfer to the soil. Such conditions increase the likelihood of ecologically significant heating that can affect root systems, soil biota, and post-fire regeneration dynamics. In contrast, the weaker directional contrast observed in Malacatos is consistent with a setting where fuel traits and landscape structure promote more rapid heat dissipation or more homogeneous combustion patterns, leading to reduced contrasts in belowground thermal impact. Together, these findings support interpreting soil heating as a component of fire severity whose controlling mechanisms vary with elevation, vegetation composition, and fuel-bed structure (Keeley 2009; Santín and Doerr 2016).

Differential vulnerability of Andean ecosystems to fire

The ecological consequences of the observed altitudinal differences in fire behavior are unlikely to be uniform because Andean ecosystems vary in resilience mechanisms, recovery rates, and sensitivity to repeated burning. Along the studied gradient, differences in vegetation structure and functional imply that similar fire-weather conditions can translate into contrasting ecological outcomes. The relative dominance of pyrophytic, fire-resistant, or fire-sensitive species influences fuel flammability, combustion duration, and the likelihood that heat penetrates the soil, thereby shaping post-fire impacts on belowground processes and regeneration dynamics. In high-elevation páramo-type systems, where steep terrain, wind exposure, and recurrent anthropogenic ignitions interact, repeated burning may shift vegetation structure and alter long-term recovery trajectories (Díaz et al. 2023; Pausas and Keeley 2021). Under these conditions, fire behavior that promotes sustained flame residence and greater soil heating can affect root systems, soil biota, and nutrient cycling, potentially slowing recovery and modifying species composition. Evidence from southern Ecuador indicates that post-fire responses are strongly conditioned by local bioclimatic context and vegetation type, supporting a zone-specific interpretation of vulnerability rather than a single generalized mechanism (Díaz et al. 2023; Arcos et al. 2023).

At mid elevations, where fire activity may be more episodic and moisture constraints more variable, vulnerability may be closely tied to climatic fluctuations that periodically relax fuel moisture limitations. In these systems, years with extended dry periods may allow fires to behave more like those typical of wind-exposed highlands, increasing the likelihood of ecologically significant impacts. Soil temperature after the fire was accurately modeled using the burning pattern, wind direction, and the NDVI spectral index, which measures gross photosynthetic vigor. This suggests that vulnerability is not constant but dynamically linked to interannual climate variability and vegetation water status.

At lower elevations, vulnerability may be expressed less through consistently high fire intensity and more through landscape configuration and land-use history. Fragmentation and agricultural expansion can reduce mature fuel continuity while increasing ignition pressure, producing patchy burn mosaics that complicate recovery and management (Tapia-Armijos et al. 2015; Radeloff et al. 2023). In such settings, vegetation composition can condition outcomes by favoring fuel types that either promote rapid, flashy combustion (limiting sustained soil heating) or maintain longer residence times under certain configurations, thereby decoupling aboveground fire behavior from belowground thermal effects. As a result, ecological vulnerability at lower elevations may be best understood as socio-ecological, mediated not only by biophysical fire behavior but also by human-driven ignition patterns and the spatial arrangement of fuels (Pausas and Keeley 2021; Radeloff et al. 2023).

These patterns indicate that the elevation gradient is associated with shifts not only in fire behavior but also in the mechanisms of ecosystem vulnerability. From higher-elevation systems, where terrain and wind can amplify fire impacts on soils and vegetation, to lower-elevation landscapes, where fragmentation and ignition pressure shape heterogeneous fire effects, vulnerability emerges as the product of interacting ecological and social drivers. Recognizing these differences is essential for anticipating post-fire recovery trajectories and for designing management strategies tailored to the specific fire behavior regimes of Andean socio-ecological systems.

Regional context and comparison with other mountainous ecosystems

Placed within the broader mountain-fire literature, these findings reinforce the idea that elevation acts as a surrogate for shifting combinations of fuels, microclimate, and topographic forcing that shape fire behavior across mountain systems (Veblen 2008; Povak et al. 2018). Similar patterns have been described in other mountain regions where terrain-driven winds and slope interact with vegetation structure to create strong local variability in fire spread and flame development, while broader climate and land use conditions regulate when fuels become flammable (Povak et al. 2018; Pausas and Keeley 2021). In the Andes, such interactions are further complicated by long histories of human ignitions and land transformation, which modulate fuel continuity and exposure across elevation bands (Armenteras et al. 2021; Díaz et al. 2023). In this context, an altitudinal framework is not only a geographic descriptor but an ecological one, reflecting shifts in the dominant controls of fire behavior. Higher elevations tend to be more influenced by wind–slope coupling and terrain exposure, mid elevations by moisture limitations and interannual climatic variability, and lower elevations by land-use legacies and fragmented fuel structure. Recognizing these differences supports a zone-specific interpretation of fire dynamics rather than a single generalized mechanism across the Andean landscape (Veblen 2008; Pausas and Keeley 2021).

Implications for integrated fire management in the Andes

Because the dominant controls of fire behavior shift with elevation and landscape context, management strategies are more effective when framed as Integrated Fire Management (IFM) adapted to ecological zones rather than as a uniform, suppression-centric approach (Pausas and Keeley 2021; Correa-Quezada et al. 2025). In higher-elevation systems where wind exposure and slope can promote rapid fire spread and sustained flame residence, preparedness may need to emphasize early detection under windy conditions and protection of areas where soil heating could have long-term ecological consequences. At mid elevations, where fire activity may be strongly modulated by seasonal and interannual moisture variability, monitoring vegetation water status can help anticipate periods when moisture-limited systems typically become more flammable. In lower-elevation, fragmented landscapes, management may benefit from focusing on fuel connectivity, ignition prevention, and the spatial arrangement of vegetation, as fire behavior in these areas can be highly heterogeneous and strongly influenced by human land use (Tapia-Armijos et al. 2015; Radeloff et al. 2023).

Early-warning systems that integrate meteorological drivers (particularly wind and atmospheric dryness) with remote sensing indicators of vegetation water status (e.g., NDMI) can help identify windows of increased fire potential across elevation zones (Yebra et al. 2013; Díaz et al. 2023). This approach is especially relevant in regions where expanding wildland–urban interfaces and frequent human ignitions increase exposure, making risk reduction dependent not only on fire suppression capacity but also on land-use planning and community engagement (Radeloff et al. 2023; Veloso et al. 2025). Finally, considering the potential for rare but high-impact events is important, even in landscapes dominated by human-caused ignitions. Compound conditions (such as strong wind episodes coinciding with drought and sufficient fuel continuity) can generate fires with behavior that exceeds typical local experience and suppression capacity (Tedim et al. 2018; Pausas and Keeley 2021). Within the Andes context, IFM therefore benefits from combining community-based ignition prevention and training with targeted risk reduction in high-exposure areas, while maintaining monitoring frameworks capable of tracking fire effects on vegetation and soil across ecological zones (Certini 2005; Santín and Doerr 2016).

Conclusions

The indicators modeled in this paper served to quantify fire behavior and its physical impact, making it possible to determine the difficulty of controlling the fire, the level of damage to forest structure and the degree of biological alteration of the soil. Fire behavior along the Andean elevation gradient was shaped by interacting controls of topography, atmospheric conditions, and vegetation structure, demonstrating that elevation reorganizes the mechanisms governing fire spread and flame development rather than imposing a single dominant driver. At higher elevations, steep slopes and greater wind exposure favored stronger wind–slope coupling, creating conditions that can promote rapid fire spread and sustained flame development, with greater potential for soil heating. At mid elevations, vegetation moisture emerged as a key ecological constraint, indicating that fire activity in these zones may be particularly sensitive to short-term drying and interannual climatic variability. In contrast, lower-elevation systems were more strongly influenced by fuel structure, land-use legacies, and surface desiccation, leading to more spatially heterogeneous fire behavior dependent on fine-scale fuel connectivity.

These altitudinal differences imply that the ecological impacts of fire, particularly those related to soil heating, vegetation mortality, and post-fire recovery, are also likely to vary systematically across the gradient. Fire behavior in exposed high-Andean environments may more readily translate into belowground thermal effects that influence soil biota and nutrient dynamics, whereas in lower-elevation, fragmented landscapes, fire effects may be patchier and more mediated by human-modified fuel mosaics. Intermediate zones may experience episodic shifts in fire behavior when moisture limitations are relaxed, linking ecological vulnerability to climatic variability. Models developed in these latter areas emphasized that vegetation water content is a key predictor, but its explanatory power is concentrated in vertical dynamics, while lateral fire spread requires additional predictors linked to fuel structure and wind variability.

By identifying how the dominant controls of fire behavior shift with elevation, this study highlights the importance of interpreting wildfire dynamics within their ecological and topographic context. These findings support the development of Integrated Fire Management strategies that recognize differences in fire behavior regimes across Andean landscapes, linking prevention, monitoring, and post-fire assessment to the specific ecological processes that govern fire impacts in each zone. Grounding fire governance in an understanding of these biophysical drivers can improve the anticipation of fire effects on soils, vegetation, and ecosystem services under changing climatic and land-use conditions. Future work should integrate multi-sensor spectral metrics with fine-scale fuel metrics and enhance transferability under a changing climate (Huang et al. 2025; Tutland et al. 2025; Tsallis et al. 2025).

Supplementary Information

The online version contains supplementary material available at https://doi.org/10.1186/s42408-026-00470-y.

Additional file 1: Table S1. Normal weather conditions, meteorological variables during experimental burns, and physiographic characteristics of the three study zones along the elevational gradient in Loja canton, southern Ecuador. Table S2. Spectral indices extracted from Sentinel-2 used for the assessment of vegetation cover, moisture stress, and soil conditions. Table S3. Post-fire soil temperature response to burning pattern by study zone. Fig. S1. Scatter plots of PCA using the first two principal components (PC1 and PC2) computed from: air temperature, solar radiation, wind speed, wind direction, relative humidity, slope, altitude, sine of the wind direction (sin(Wind Dir.)) and $\cos\left(\widehat{\overrightarrow{WD} - \overrightarrow{BP}}\right)$ x wind speed. Fig. S2 Box and whisker plots of ARVI, GNDVI, NDMI in the three study zones. Scatter plot using the first two principal components calculated with the spectral variables defined in Table S2. References used in supplementary material.

Acknowledgements
The authors thank the support of the project entitled, Monitoring of areas susceptible to forest fires and priority prevention areas of the Loja canton, with code No. 46-DI-FARNR-2023, from the Universidad Nacional de Loja. Angel Balaguer-Beser thanks the support received through the grant PID2024-158591OB-I00, funded by MICIU/AEI/10.13039/501100011033 and the European Social Fund Plus (ESF+).

Authors' contributions
FG, CGC, VCP and OJS conceived and designed the study and the prescribed burns. FG organized and oversaw data collection. ABB and CGC analyzed the data and developed the analysis approach and validation. ABB, FG, CGC and VPC made figures and tables. OJS was in charge of project administration. All authors participated in the writing and review of the manuscript. All authors read and approved of the final manuscript.

Funding
This research was carried out with the financial support of the Universidad Nacional de Loja in the frame of project 46-DI-FARNR-2023.This research has been supported by the grant PID2024-158591OB-I00, funded by MICIU/AEI/10.13039/501100011033 and the European Social Fund Plus (ESF+).

Data availability
The datasets used and analyzed during the current study are available from the corresponding author on reasonable request.

Declarations

Ethics approval and consent to participate
Not applicable.

Consent for publication
Not applicable.

Competing interests
The authors declare no competing interests.

Author details
[1]Geo-Environmental Cartography and Remote Sensing Group (CGAT-UPV), Universitat Politècnica de València, Camí de Vera S/N, 46022 València, Spain. [2]Dirección de Investigación, Centro de Investigaciones Territoriales, Universidad Nacional de Loja (UNL), Ciudadela Universitaria Guillermo Falconí Espinosa, Loja 110101, Ecuador. [3]Universidad Nacional de Loja (UNL), Facultad Agropecuaria y de Recursos Naturales Renovables, Carrera de Ingeniería Ambiental, Grupo de Investigación de Medio Ambiente y Recursos Naturales, Ciudadela Universitaria Guillermo Falconí Espinosa, Loja 110101, Ecuador. [4]Departamento de Ciencias Biológicas y Agropecuarias, Universidad Técnica Particular de Loja, San Cayetano Alto S/N, Loja 1101608, Ecuador. [5]Universidad Nacional de Loja (UNL), Facultad Agropecuaria y de Recursos Naturales Renovables, Carrera de Ingeniería Forestal, Centro de Investigaciones Territoriales,, Ciudadela Universitaria Guillermo Falconí Espinosa, Loja 110101, Ecuador.

Received: 14 February 2026 Accepted: 4 March 2026
Published online: 23 March 2026

References

Arcos, M. A., R. Edo-Botella, A. Balaguer-Beser, and L. A. Ruiz. 2023. Analyzing independent LFMC empirical models in the mid-Mediterranean region of Spain attending to vegetation types and bioclimatic zones. *Forests* 14 (7): 1299. https://doi.org/10.3390/f14071299.

Argañaraz, J. P., A. M. Cingolani, L. M. Bellis, and M. A. Giorgis. 2020. Fire incidence along an elevation gradient in the mountains of central Argentina. *Ecología Austral* 30:268–281.

Argibay, D. S., and D. Renison. 2018. Effect of fire and livestock on *Polylepis australis* (Rosaceae) woodlands along an altitudinal gradient in the mountains of central Argentina. *Bosque (Valdivia)* 39 (1): 145–150.

Armenteras, D., N. Rodríguez, and J. Retana. 2013. Landscape dynamics in northwestern Amazonia: An assessment of pastures, fire and illicit crops as drivers of tropical deforestation. *PLoS ONE* 8 (1): e54310.

Armenteras, D., L. M. Dávalos, J. S. Barreto, A. Miranda, A. Hernández-Moreno, C. Zamorano-Elgueta, T. M. González-Delgado, M. C. Meza-Elizalde, and D. Retana. 2021. Fire-induced loss of the world's most biodiverse forests in Latin America. *Science Advances* 7 (33): eabd3357. https://doi.org/10.1126/sciadv.abd3357.

Barros, A., A. Ager, M. Day, M. Krawchuk, and T. Spies. 2018. Wildfires managed for restoration enhance ecological resilience. *Ecosphere* 9:e02161. https://doi.org/10.1002/ecs2.2161.

Bekker, M. F., and A. H. Taylor. 2001. Gradient analysis of fire regimes in montane forests of the southern Cascade Range, Thousand Lakes Wilderness, California, USA. *Plant Ecology* 155 (1): 15–28. https://doi.org/10.1023/A:1013263212092.

Bridge, S. R. J., K. Miyanishi, and E. A. Johnson. 2005. A critical evaluation of fire suppression effects in the boreal forest of Ontario. *Forest Science* 51 (1): 41–50. https://doi.org/10.1093/forestscience/51.1.41.

Brooks, J.R., and S.B. Jack. 2018. Longleaf pine: restoration or reforestation? 19th Biennial Southern Silvicultural Research Conference 1: 303–308. https://www.srs.fs.usda.gov/pubs/gtr/gtr_srs234/gtr_srs234-45.pdf

Camprubí, À. C., P. González-Moreno, and V. R. de Dios. 2022. Live fuel moisture content mapping in the Mediterranean Basin using random forests and combining MODIS spectral and thermal data. *Remote Sensing* 14 (13): 3162. https://doi.org/10.3390/rs14133162.

Cangelosi, R., and A. Goriely. 2007. Component retention in principal component analysis with application to cDNA microarray data. *Biology Direct* 2:2. https://doi.org/10.1186/1745-6150-2-2.

Carrión-Paladines, V., M. B. Hinojosa, L. Jiménez Álvarez, F. Reyes-Bueno, L. Correa Quezada, and R. García-Ruiz. 2022. Effects of the severity of wildfires on some physical-chemical soil properties in a humid montane scrublands ecosystem in Southern Ecuador. *Fire* 5 (3): 66. https://doi.org/10.3390/fire5030066.

Carrión-Paladines, V., A. Fríes, M. B. Hinojosa, A. Oña, L. Jiménez-Álvarez, Á. Benítez, F. López-Rodríguez, and R. García-Ruiz. 2023. Effects of low-severity fire on soil physico-chemical properties in an Andean Páramo in Southern Ecuador. *Fire* 6 (12): 447. https://doi.org/10.3390/fire6120447.

Carstens, B. C., H. N. Stoute, and N. Reid. 2010. Model selection and inference: A practical information-theoretic approach. *MOlecular Ecology* 19 (3): 620. https://doi.org/10.1111/j.1365-294X.2009.04493.x.

Celleri, R., P. Willems, W. Buytaert, and J. Feyen. 2007. Space–time rainfall variability in the Paute basin, Ecuadorian Andes. *Hydrological Processes* 21 (24): 3316–3327. https://doi.org/10.1002/hyp.6575.

Certini, G. 2005. Effects of fire on properties of forest soils: A review. *Oecologia* 143 (1): 1–10.

Coronel-Alulima, T. N. 2019. sistemas agroecológicos de la parroquia San Lucas (Loja). Prácticas resilientes ante el cambio climático. *Letras Verdes, Revista Latinoamericana De Estudios Socioambientales* 26:191–212. https://doi.org/10.17141/letrasverdes.26.2019.3806.

Correa-Quezada, L., V. Carrión-Correa, C. López, D. Segura, and V. Carrión-Paladines. 2025. Towards integrated fire management: Strengthening forest fire legislation and policies in the Andean Community of Nations. *Fire* 8 (7): 266. https://doi.org/10.3390/fire8070266.

Costa-Saura, J. M., A. Balaguer-Beser, L. A. Ruiz, J. E. Pardo-Pascual, and J. L. Soriano-Sancho. 2021. Empirical models for spatio-temporal live fuel moisture content estimation in mixed mediterranean vegetation areas using sentinel-2 indices and meteorological data. *Remote Sensing* 13 (18): 3726.

Cruz, M. G., M. E. Alexander, and M. Kilinc. 2022a. Wildfire rates of spread in grasslands under critical burning conditions. *Fire* 5 (2): 55. https://doi.org/10.3390/fire5020055.

Cruz, M. G., M. E. Alexander, and P. M. Fernandes. 2022b. Evidence for lack of a fuel effect on forest and shrubland fire rates of spread under elevated fire danger conditions: Implications for modelling and management. *International Journal of Wildland Fire* 31 (5): 471–479. https://doi.org/10.1071/WF21171.

Díaz, S. C., L. C. Quezada, L. J. Álvarez, J. Loján-Córdova, and V. Carrión-Paladines. 2023. Indigenous use of fire in the paramo ecosystem of southern Ecuador: A case study using remote sensing methods and ancestral knowledge of the Kichwa Saraguro people. *Fire Ecology* 19 (1): 5. https://doi.org/10.1186/s42408-022-00164-1.

DJI. 2023. Manual de usuario (p. 101).

Dobson, A. J., and A. G. Barnett. 2018. An Introduction to Generalized Linear Models. *Chapman and Hall/CRC*. https://doi.org/10.1201/9781315182780.

Ebrahimi, A., F. Zolfaghari, M. Ghodsi, and F. Narmashiri. 2024. Assessing the accuracy of spectral indices obtained from Sentinel images using field research to estimate land degradation. *PLoS ONE* 19 (7): e0305758. https://doi.org/10.1371/journal.pone.0305758.

Farbo, A., F. Sarvia, S. De Petris, V. Basile, and E. Borgogno-Mondino. 2024. Forecasting corn NDVI through AI-based approaches using sentinel 2 image time series. *ISPRS Journal of Photogrammetry and Remote Sensing* 211:244–261. https://doi.org/10.1016/j.isprsjprs.2024.04.011.

Fernández-Manso, A., O. Fernández-Manso, and C. Quintano. 2016. SENTINEL-2A red-edge spectral indices suitability for discriminating burn severity. *International Journal of Applied Earth Observation and Geoinformation* 50:170–175. https://doi.org/10.1016/j.jag.2016.03.005.

Flannigan, M.D., and B.M. Wotton. 2001. Climate, weather, and area burned. In: Johnson, E. A. and Miyanishi, K. (eds.). 2001. Forest fires: behavior and ecological effects. Academic Press, San Diego-San Francisco-New York-Boston-London-Sydney-Tokyo. p. 351–373.

Ganteaume, A., A. Camia, M. Jappiot, J. San-Miguel-Ayanz, M. Long-Fournel, and C. Lampin. 2013. A review of the main driving factors of forest fire ignition over Europe. *Environmental Management* 51 (3): 651–662. https://doi.org/10.1007/s00267-012-9961-z.

Geron, C., and M. Hays. 2013. Air emissions from organic soil burning on the coastal plain of North Carolina. *Atmospheric Environment* 64:192–199. https://doi.org/10.1016/j.atmosenv.2012.09.065.

Gimeno-García, E., V. Andreu, and J. L. Rubio. 2004. Spatial patterns of soil temperatures during experimental fires. *Geoderma* 118 (1–2): 17–38. https://doi.org/10.1016/S0016-7061(03)00167-8.

González, F., F. Morante-Carballo, A. González, L. Bravo-Montero, C. Benavidez-Silva, and F. Tedim. 2024. Assessment of forest fire severity for a management conceptual model: Case study in Vilcabamba, Ecuador. *Forests* 15 (12): 2210. https://doi.org/10.3390/f15122210.

Grau, H. R. 2001. Regional-scale spatial patterns of fire in relation to rainfall gradients in sub-tropical mountains, NW Argentina. *Global Ecology and Biogeography* 10 (2): 133–146. https://doi.org/10.1046/j.1466-822x.2001.00220.x.

Gutiérrez-Rodríguez, L., Y. He, M. Sun, Y. Yao, and V. de Resco- Dios. 2023. Summer compound drought-heat extremes amplify fire-weather risk and burned area beyond historical thresholds in Chongqing Region, subtropical China. *Fire* 6 (9): 346. https://doi.org/10.3390/fire6090346.

Haire, S. L., and K. McGarigal. 2009. Changes in fire severity across gradients of climate, fire size, and topography: A landscape ecological perspective. *Fire Ecology* 5 (2): 86–103. https://doi.org/10.4996/fireecology.0502086.

Hakim, L., M. Manijo, and A.A. Muliasari. 2024. Application of the NDVI and ARVI methods in measuring estimated productivity of oil palm plants using Landsat 8 Imagery at PT. Hindoli Cargill Indonesia. In BIO Web of Conferences (Vol. 123, p. 01001). EDP Sciences. https://doi.org/10.1051/bioconf/202412301001

Hakkenberg, C. R., M. L. Clark, T. Bailey, P. Burns, and S. J. Goetz. 2024. Ladder fuels rather than canopy volumes consistently predict wildfire severity even in extreme topographic-weather conditions. *Communications Earth & Environment* 5 (1): 721. https://doi.org/10.1038/s43247-024-01893-8.

Hao, B., X. Xu, F. Wu, and L. Tan. 2022. Long-term effects of fire severity and climatic factors on post-forest-fire vegetation recovery. *Forests* 13 (6): 883. https://doi.org/10.3390/f13060883.

Hofstede, R. G. 1995. The effects of grazing and burning on soil and plant nutrient concentrations in Colombian páramo grasslands. *Plant and Soil* 173 (1): 111–132. https://doi.org/10.1007/BF00155524.

Huang, K., X. Wu, L. Zhang, H. Geng, and Y. Qu. 2025. Increasing risk of global forest loss from extreme wildfires under climate change. *International Journal of Digital Earth* 18 (1): 2483982. https://doi.org/10.1080/17538947.2025.2483982.

Hueso-González, P., J. F. Martínez-Murillo, and J. D. Ruiz-Sinoga. 2018. Prescribed fire impacts on soil properties, overland flow and sediment transport in a Mediterranean forest: A 5-year study. *Science of the Total Environment* 636:1480–1489. https://doi.org/10.1016/j.scitotenv.2018.05.004.

Huete, A. R. 1988. A soil-adjusted vegetation index (SAVI). *Remote Sensing of Environment* 25 (3): 295–309. https://doi.org/10.1016/0034-4257(88)90106-X.

IUSS Working Group WRB. 2015. World Reference Base for Soil Resources 2014, Update 2015 International Soil Classification System for Naming Soils and Creating Legends for Soil Maps; World Soil Resources Reports No. 106; FAO: Rome, Italy.

Jolliffe, I. 2011. Principal Component Analysis. In: Lovric, M., ed. International Encyclopedia of Statistical Science. Springer, Berlin, Heidelberg. https://doi.org/10.1007/978-3-642-04898-2_455.

Kala, C. P. 2023. Environmental and socioeconomic impacts of forest fires: A call for multilateral cooperation and management interventions. *Natural Hazards Research* 3 (2): 286–294. https://doi.org/10.1016/j.nhres.2023.04.003.

Keating, P. L. 2007. Fire ecology and conservation in the high tropical Andes: Observations from northern Ecuador. *Journal of Latin American Geography* 6 (1): 43–62.

Keeley, J. E. 2009. Fire intensity, fire severity and burn severity: A brief review and suggested usage. *International Journal of Wildland Fire* 18 (1): 116–126. https://doi.org/10.1071/WF07049.

Kerns, B. K., M. Buonopane, W. G. Thies, and C. Niwa. 2011. Reintroducing fire into a ponderosa pine forest with and without cattle grazing: Understory vegetation response. *Ecosphere* 2 (5): 1–23. https://doi.org/10.1890/ES10-00183.1.

Kim, J. H. 2019. Multicollinearity and misleading statistical results. *Korean Journal of Anesthesiology* 72 (6): 558–569. https://doi.org/10.4097/kja.19087.

Lastovicka, J., P. Svec, D. Paluba, N. Kobliuk, J. Svoboda, R. Hladky, and P. Stych. 2020. Sentinel-2 data in an evaluation of the impact of the disturbances on forest vegetation. *Remote Sensing* 12 (12): 1914. https://doi.org/10.3390/rs12121914.

Lippok, D., S. G. Beck, D. Renison, S. C. Gallegos, F. V. Saavedra, I. Hensen, and M. Schleuning. 2013. Forest recovery of areas deforested by fire increases with elevation in the tropical Andes. *Forest Ecology and Management* 295:69–76. https://doi.org/10.1016/j.foreco.2013.01.011.

Liu, Y., J. Qian, and H. Yue. 2021. Comprehensive evaluation of Sentinel-2 red edge and shortwave-infrared bands to estimate soil moisture. *IEEE Journal of Selected Topics in Applied Earth Observations and Remote Sensing* 14:7448–7465. https://doi.org/10.1109/JSTARS.2021.3098513.

Mangewa, L. J., P. A. Ndakidemi, R. D. Alward, H. K. Kija, J. K. Bukombe, E. R. Nasolwa, and L. K. Munishi. 2022. Comparative assessment of UAV and sentinel-2 NDVI and GNDVI for preliminary diagnosis of habitat conditions in Burunge wildlife management area, Tanzania. *Earth* 3 (3): 769–787. https://doi.org/10.3390/earth3030044.

Mhawej, M., G. Faour, and J. Adjizian-Gerard. 2015. Wildfire likelihood's elements: A literature review. *Challenges* 6 (2): 282–293. https://doi.org/10.3390/challe6020282.

Municipio de Loja. 2014. *Plan de Desarrollo y Ordenamiento Territorial. Fase I Diagnóstico*, vol. 20. Loja, Ecuador: Municipio de Loja.

Muñoz-Rojas, M., W. Lewandrowski, T. E. Erickson, K. W. Dixon, and D. J. Merritt. 2016. Soil respiration dynamics in fire affected semi-arid ecosystems: Effects of vegetation type and environmental factors. *Science of the Total Environment* 572:1385–1394. https://doi.org/10.1016/j.scitotenv.2016.02.086.

Nelson, R. M. 2002. An effective wind speed for models of fire spread. *International Journal of Wildland Fire* 11 (2): 153–161. https://doi.org/10.1071/WF02031.

Ochoa-Cueva, P., A. Fries, P. Montesinos, J. A. Rodríguez-Díaz, and J. Boll. 2015. Spatial estimation of soil erosion risk by land-cover change in the Andes of southern Ecuador. *Land Degradation & Development* 26 (6): 565–573. https://doi.org/10.1002/ldr.2219.

Oñate-Valdivieso, F., A. Fries, K. Mendoza, V. Gonzalez-Jaramillo, F. Pucha-Cofrep, R. Rollenbeck, and J. Bendix. 2018. Temporal and spatial analysis of precipitation patterns in an Andean region of southern Ecuador using LAWR weather radar. *Meteorology and Atmospheric Physics* 130 (4): 473–484. https://doi.org/10.1007/s00703-017-0535-8.

Paladines, S. 2013. *Vulnerabilidad a Nivel Municipal del Cantón Loja*. Loja, Ecuador: CEDIA.

Pausas, J. G., and J. E. Keeley. 2021. Wildfires and global change. *Frontiers in Ecology and the Environment* 19 (7): 387–395. https://doi.org/10.1002/fee.2359.

Piepho, H. P. 2004. An algorithm for a letter-based representation of all-pairwise comparisons. *Journal of Computational and Graphical Statistics* 13 (2): 456–466. https://doi.org/10.1198/1061860043515.

Povak, N. A., P. F. Hessburg, and R. B. Salter. 2018. Evidence for scale-dependent topographic controls on wildfire spread. *Ecosphere* 9 (10): e02443. https://doi.org/10.1002/ecs2.2443.

Radeloff, V. C., M. H. Mockrin, D. Helmers, A. Carlson, T. J. Hawbaker, S. Martinuzzi, F. Schug, P. M. Alexandre, H. A. Kramer, and A. M. Pidgeon. 2023. Rising wildfire risk to houses in the United States, especially in grasslands and shrublands. *Science* 382 (6671): 702–707. https://doi.org/10.1126/science.ade9223.

Ren, H., G. Zhou, and F. Zhang. 2018. Using negative soil adjustment factor in soil-adjusted vegetation index (SAVI) for aboveground living biomass estimation in arid grasslands. *Remote Sensing of Environment* 209:439–445. https://doi.org/10.1016/j.rse.2018.02.068.

Robinne, F. N., and F. Secretariat. 2021. Impacts of disasters on forests, in particular forest fires. *UNFFS Background paper*.

Rocha, D. R., F. L. Melquiades, and E. L. Thomaz. 2019. Modeling the soil burn effect for temperature prediction by energy dispersive X ray Fluorescence in an haplic cambisol soil. *Applied Radiation and Isotopes* 150:26–30. https://doi.org/10.1016/j.apradiso.2019.05.012.

Rollenbeck, R., and J. Bendix. 2011. Rainfall distribution in the Andes of southern Ecuador derived from blending weather radar data and meteorological field observations. *Atmospheric Research* 99 (2): 277–289. https://doi.org/10.1016/j.atmosres.2010.10.018.

Román-Cuesta, R. M., C. Carmona-Moreno, G. Lizcano, M. New, M. Silman, T. Knoke, Y. Malhi, I. Oliveras, H. Asbjornsen, and M. Vuille. 2014. Synchronous fire activity in the tropical high Andes: An indication of regional climate forcing. *Global Change Biology* 20 (6): 1929–1942. https://doi.org/10.1111/gcb.12538.

Rossa, C. G., D. A. Davim, Â. Sil, and P. M. Fernandes. 2024. Field-based generic empirical flame length–fireline intensity relationships for wildland surface fires. *International journal of wildland fire* 33 (1): WF23127. https://doi.org/10.1071/WF23127.

Santín, C., and S. H. Doerr. 2016. Fire effects on soils: The human dimension. *Philosophical Transactions of the Royal Society b: Biological Sciences* 371 (1696): 20150171. https://doi.org/10.1098/rstb.2015.0171.

Silva, J., J. Marqués, I. Gonçalves, R. Brito, S. Teixeira, J. Teixeira, and F. Alvelos. 2022. A systematic review and bibliometric analysis of wildland fire behavior modeling. *Fluids* 7 (12): 374. https://doi.org/10.3390/fluids7120374.

Storey, M. A., O. F. Price, M. Almeida, C. Ribeiro, R. A. Bradstock, and J. J. Sharples. 2021. Experiments on the influence of spot fire and topography interaction on fire rate of spread. *PLoS ONE* 16 (1): e0245132. https://doi.org/10.1371/journal.pone.0245132.

Sullivan, A. L. 2009. Wildland surface fire spread modelling, 1990–2007. 1: Physical and quasi-physical models. *International Journal of Wildland Fire* 18 (4): 349–368. https://doi.org/10.1071/WF06143.

Tapia-Armijos, M. F., J. Homeier, C. I. Espinosa, C. Leuschner, and M. De La Cruz. 2015. Deforestation and forest fragmentation in South Ecuador since the 1970s–losing a hotspot of biodiversity. *PLoS ONE* 10 (9): e0133701. https://doi.org/10.1371/journal.pone.0133701.

Tedim, F., V. Leone, M. Amraoui, C. Bouillon, M. R. Coughlan, G. M. Delogu, P. M. Fernandes, C. Ferreira, S. McCaffrey, T. K. McGee, J. Parente, D. Paton, M. G. Pereira, L. M. Ribeiro, D. X. Viegas, and G. Xanthopoulos. 2018. Defining extreme wildfire events: Difficulties, challenges, and impacts. *Fire* 1 (1): 9. https://doi.org/10.3390/fire1010009.

Tsallis, C., P. Papageorgas, S. Dellagi, D. Piromalis, G. Vokas, and A. Belhadi. 2025. Satellite remote sensing for post-fire recovery: sustainable reforestation using NDVI, LST and SMI. *Management of Environmental Quality: An International Journal: 1–14*. https://doi.org/10.1108/MEQ-03-2025-0187

Tutland, N. J., A. P. Wion, C. J. May, G. C. Hutchings, H. A. Nowak, J. R. Gattiker, J. K. Hiers, R. R. Linn, S. M. Pokswinski, and E. Q. Margolis. 2025. Representing 3-dimensional fuels for physics-based fire behavior models: A general framework and case study in a type-converted post-fire shrubfield. *Fire Ecology* 21 (1): 43. https://doi.org/10.1186/s42408-025-00383-2.

Veblen, K. E. 2008. *Livestock and wildlife effects on the successional development of a savanna landscape mosaic in East Africa*. Davis: University of California.

Veloso, F., P. Souza-Alonso, and G. Saiz. 2025. Improving wildfire resilience in the Mediterranean Central-South Regions of Chile. *Fire* 8 (6): 212. https://doi.org/10.3390/fire8060212.

Waldrop, T.A., and S.L. Goodrick. 2012. Introduction to prescribed fires in Southern ecosystems. USDA Forest Service, Southern Research Station. *Science Update SRS-054*.

Wood, S. N. 2011. Fast stable restricted maximum likelihood and marginal likelihood estimation of semiparametric generalized linear models. *Journal of the Royal Statistical Society. Series b, Statistical Methodology* 73 (1): 3–36. https://doi.org/10.1111/j.1467-9868.2010.00749.x.

Yebra, M., P. E. Dennison, E. Chuvieco, D. Riaño, P. M. Zylstra, Jr. . Hunt, F. M. Danson, Y. Qi, and S. Jurdao. 2013. A global review of remote sensing of live fuel moisture content for fire danger assessment: Moving towards operational products. *Remote Sensing of Environment* 136:455–468. https://doi.org/10.1016/j.rse.2013.05.029.

Zapata-Ríos, X., C. Lopez-Fabara, A. Navarrete, S. Torres-Paguay, and M. Flores. 2021. Spatiotemporal patterns of burned areas, fire drivers, and fire probability across the equatorial Andes. *Journal of Mountain Science* 18:952–972. https://doi.org/10.1007/s11629-020-6402-y.

Zhu, Y., S. Zhao, Y. Zhang, C. Zhang, and J. Wu. 2024. A review of statistical-based fault detection and diagnosis with probabilistic models. *Symmetry* 16 (4): 455. https://doi.org/10.3390/sym16040455.

Publisher's Note